RSS Distribution-Based Passive Localization and Its Application in Sensor Networks

Chen Liu, Dingyi Fang, Zhe Yang, Hongbo Jiang, *Senior Member, IEEE*, Xiaojiang Chen, *Member, IEEE*, Wei Wang, Tianzhang Xing, and Lin Cai, *Senior Member, IEEE*

Abstract—Passive localization is fundamental for many applications such as activity monitoring and real-time tracking. Existing received signal strength (RSS)-based passive localization approaches have been proposed in the literature, which depend on dense deployment of wireless communication nodes to achieve high accuracy. Thus, they are not cost-effective and scalable. This paper proposes the RSS distribution-based localization (RDL) technique, which can achieve high localization accuracy without dense deployment. In essence, RDL leverages the RSS and the diffraction theory to enable RSS-based passive localization in sensor networks. Specifically, we analyze the fine-grained RSS distribution properties at a variety of node distances and reveal that the structure of the triangle is efficient for low-cost passive localization. We further construct a unit localization model aiming at high accuracy localization. Experimental results show that RDL can improve the localization accuracy by up to 50%, compared to existing approaches when the error tolerance is less than 1.5 m. In addition, we apply RDL to facilitate the application of moving trajectory identification. Our moving trajectory identification includes two phases: an offline phase where the possible locations can be estimated by RDL and an online phase where we precisely identify the moving trajectory. We conducted extensive experiments to show its effectiveness for this application—the estimated trajectory is close to the ground truth.

Index Terms—Passive object localization, RSS distribution, WSNs.

C. Liu, D. Fang, X. Chen, and T. Xing are with the School of Information Science and Technology, Northwest University, Xi'an 710127, China (e-mail: liuchen@nwu.edu.cn; dfy@nwu.edu.cn; xjchen@nwu.edu.cn; xtz@nwu.edu.cn).

Z. Yang is with the School of Computer Science, Northwestern Polytechnical University, Xi'an 710129, China (e-mail: zyang@nwpu.edu.cn).

H. Jiang is with the School of Electronic Information and Communications, Huazhong University of Science and Technology, Wuhan 430074, China (e-mail: hongbojiang2004@gmail.com).

W. Wang is with the School of Electronics and Information, Northwestern Polytechnical University, Xi'an 710129, China, and also with the School of Information Science and Technology, Northwest University, Xi'an 710127, China (e-mail: wwang@nwu.edu.cn).

L. Cai is with the Department of Electrical and Computer Engineering, University of Victoria, Victoria, BC, Canada (e-mail: cai@ece.uvic.ca).

Color versions of one or more of the figures in this paper are available online at http://ieeexplore.ieee.org.

I. INTRODUCTION

LOCALIZATION in sensor networks has been playing a key role in many applications, such as geographic routing and position-aware data processing. Most of the existing localization technologies [1]–[11] request that the objects/users carry communication-capable devices to send/receive electromagnetic waves, acoustic or ultrasonic signals, etc. By doing so, they can be detected and then located by the anchor nodes. Despite their success in many scenarios, these approaches become infeasible in some circumstances, such as intrusion detection and wildlife monitoring, where equipping each object with communication devices would be extremely expensive or even impossible. Recently, a growing interest has been shown in the passive, device-free localization techniques [12]–[24] that do not rely on carry-on devices.

Compared with other passive localization techniques, such as GPS and CSI (Channel State Information) [25], which need some special devices (e.g., the extra video [26], infrared sensors or the Intel 5300 network card), the Received Signal Strength (RSS)-based passive localization technologies are widely used because of their low-cost infrastructure. These technologies rely on an array of nodes to communicate with each other and to measure the RSS values. The basic idea is to exploit the disturbance of the object due to its presence in the radio environment [12], to estimate its location without relying on any carry-on devices. These approaches typically locate objects using a dense deployment of sensor nodes [13], [18], [19] and the localization accuracy depends on the deployment density and distance between sensor nodes. In general, the denser the sensors, the higher the tracking accuracy. However, a dense deployment of sensors results in a high cost for the equipment and the communication, particularly in a large region.

To solve this problem, some researchers have used compressive sensing (CS) technique [20] to locate the object in a sparse deployment scenario. However, the complexity of the reconstruction algorithm in CS is high and the solution is sensitive to environmental noise. In this paper, we present a novel RSS Distribution-Based Localization (RDL) technique that provides sufficient accuracy even with sparse deployment, and for a low cost. Specifically, we investigate the RSS distribution properties of the communication links based on intensive measurement and the diffraction theory to enable high accuracy. To this end, we analyze the fine-grained RSS distribution properties of a single link at a variety of node distances that confirm the signal symmetry properties. Based on the properties, we obtain the exact location by matching the RSS values and the distribution

properties. Then we show that the structure of the triangle to deploy the nodes is efficient for low-cost passive localization. We further construct a Unit Localization Model (ULM) for high accuracy localization. Our results show that the localization accuracy is improved by up to 50% when the error tolerance is less than 1.5 m, compared to existing approaches [13]. In addition, RDL can leverage its ability to enable a passive RSS-based tracking application. The average tracking error is 0.59 m when the node distance is 4 m.

The main contributions of this paper are as follows:

- We investigate the RSS distribution properties based on extensive measurements and the diffraction theory. We can obtain high localization accuracy by matching the RSS values and the distribution properties without dense deployment.
- We propose an inexpensive, real-time and efficient passive localization approach called RDL. Our numerical results show that RDL improves the localization accuracy by up to 50% when the error tolerance is less than 1.5 m, compared to the Midpoint algorithm and the Intersection algorithm in [13]. We verify the proposed approach by both trace-driven simulation and implementation on a testbed. While our design and results are presented in the context of sensor networks, the basic idea can be extended to other systems, such as Wi-Fi.
- We further apply RDL to track the moving object, which includes three steps. The first step is to eliminate the environment noise in the obtained RSS vector. The second step is to identify the so-called effective contribution nodes. Third, a series of estimated locations are used to identify the trajectory.

The rest of this paper is organized as follows: Section II introduces the related work. The signal symmetry properties are proposed in Section III. The localization approach based on the Unit Localization Model and experimental results are presented in Section IV. Section V presents a tracking application and the performance evaluation. Concluding remarks are given in Section VI.

II. RELATED WORKS

Active Object Localization: A number of RF-based localization systems have been proposed in the literature [1]–[7]. LANDMARC [1] is a location sensing prototype that uses the Radio Frequency Identification (RFID) technology for indoor localizations. The location of the tracked object is estimated based on the K nearest reference tags, where the object is required to carry an RFID tag. MoteTrack is another system to locate the mobile nodes and the location of each mobile node is obtained by the RSS signatures from several anchor nodes, where the signature database is stored in anchor nodes [4]. RADAR [3] operates by combining signal strength information at multiple base stations based on empirical measurements. FreeLoc [8] is an efficient localization method addressing three major technical issues posed in crowdsourcing-based systems. It provides consistent localization accuracy in an environment where the device heterogeneity and the multiple surveyor problems exist. Recently, Wang *et al.* [9] proposed a fine-grained

RFID positioning system that is robust to multipath and non-line-of-sight scenarios. Results show that their design can locate misplaced books with a median accuracy of 11 cm. Yang *et al.* [27] proposed a RFID-based system, Tagoram, for object localization and tracking with the accuracy in mm. Nevertheless, these localization algorithms request that the object should carry a communication-capable device (transmitter and/or a receiver), which is not feasible in situations like intrusion detection and wildlife monitoring.

Passive Object Localization: In [17], the proposed solution does not require the object to carry any wireless devices, while the RSS was used instead. However, their system can only detect the presence of the object but cannot give the exact locations. In [13], [18], [19], a signal dynamic model based on RSS was proposed to locate the transceiver-free objects. The anchor nodes are deployed as a grid array and the distance between nodes is 1 m or 2 m. The objects can be passively located, but dense deployment may not be feasible for covering a large region due to the high communication cost and the equipment investment. Another passive localization approach was proposed in [14], but it needs to increase the number of sensors to obtain high accuracy, which is also not scalable. To cope with objects moving at dynamic speeds, [21] proposed an adaptive speed change detection framework, but a dense deployment is still needed. Wang *et al.* [20] proposed a multi-object passive localization method based on compressive sensing, which does not depend on dense deployment. In any case, they ignored the complexity of the reconstruction algorithm while using a compressive sensing technique. This paper presents a novel passive localization approach — RDL. Instead of the coarse-grained RF-disturbance by the object, we exploit the fine-grained RSS distribution properties. We reveal the Signal Symmetry Properties and construct the Unit Localization Model to provide high localization accuracy in a sparse deployment. Furthermore, we leverage the RDL ability to enable a passive tracking application to identify the trajectory of the moving object.

III. SIGNAL SYMMETRY PROPERTIES

To exploit the fine-grained RSS distribution, we first investigate the RSS distribution properties. For the sake of convenience, in this section, we start with a simple case of one single link.

In Fig. 1, the monitoring area is divided into four parts by the line-of-sight (LOS) (X-axis) and its perpendicular (Y-axis). We define each parallel line of the Y-axis as a y-line. Furthermore, we divide the area into s × t grids. When an object moves into the monitoring area, as shown in Fig. 1, it affects the RF signals between the transmitter **T** and the receiver **R**. For a single link with an object at different locations, the important signal symmetry properties (SSPs) can be seen, as summarized below:

1) SSP1: The RSS values vary as the object appears in different grids;
2) SSP2: The RSS values are almost the same when the object appears in a pair of symmetrical grids about the area center;
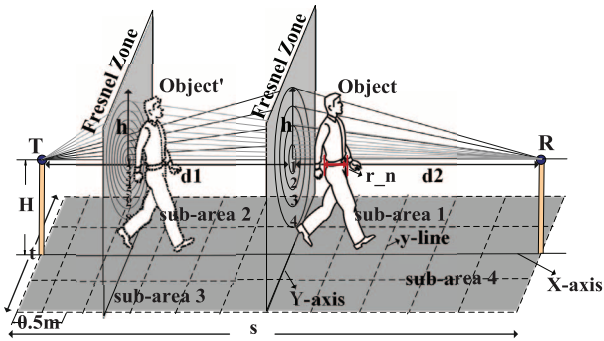3) SSP3: The affected area of one single link is quite limited.

Fig. 1. The monitoring area of a single link is divided into four parts by the X-axis and the Y-axis. Then, we model the SSPs using the knife-edge diffraction model. When the object appears at different places, it will block the different number of Fresnel zones and affect the RF signals of the transceiver pair.

A. Theoretical Foundations

According to the diffraction theory [28], we model the signal propagation properties using the knife-edge diffraction model when the transceivers are deployed in a line. Here, we refer to the *diffraction pattern* as the RSS distribution of a single link caused by an object. It is formed due to the RSS attenuation caused by diffraction of radio wave when the object block the signal [28]. By doing so, it is convenient to calculate the theoretical diffraction pattern based on the following equations (Eq. (1) to Eq. (5)). Let the width of the object be r_n, which can be calculated by the radius of Fresnel zone circle equation [28] as follows:

$$r_n = \sqrt{\frac{n\lambda d_1 d_2}{d_1 + d_2}}, \tag{1}$$

where n refers to the number of Fresnel zones affected by the object. Specifically, Fresnel zones represent successive regions where secondary waves have a path length from the transmitter to receiver which is $n\lambda/2$ greater than the total length of a LOS path [28]. The concentric circles in Fig. 1 show an example of Fresnel zones. Furthermore, the larger the number of Fresnel zones, the larger the RSS attenuation. Let λ be the wavelength, d_1 be the distance between the transmitter and the object, and d_2 be the distance between the object and the receiver. Equivalently, n can be given by:

$$n = \frac{r_n^2(d_1 + d_2)}{\lambda d_1 d_2}. \tag{2}$$

Apparently, n varies with changes of d_1 and d_2, which means that when an object stays at different grids (different d_1 and d_2), it can affect the different number of Fresnel zones. Accordingly, we can observe a variety of RSS values when an object stays at different grids. That is, SSP1 holds.

If an object does not block the area of the first Fresnel zone [28], the diffraction loss will be quite trivial. As a rule of thumb [28], as long as 55% or more of the first Fresnel zone is not blocked, further Fresnel zone clearance does not significantly mitigate the diffraction loss. That is, SSP3 holds.

The Fresnel-Kirchoff diffraction parameter v is given by [28]:

$$v = h\sqrt{\frac{2(d_1 + d_2)}{\lambda d_1 d_2}}, \tag{3}$$

where h is the effective height of the object. The electric field strength, E_d, of a knife-edge diffracted wave is given by

$$\frac{E_d}{E_0} = F(v) = \frac{1+j}{2} \int_v^\infty exp\left(\frac{-j\pi t^2}{2}\right) d_t, \tag{4}$$

where E_0 is the free space field strength and $F(v)$ is the complex Fresnel integral. $F(v)$ is a function of the Fresnel-Kirchoff diffraction parameter v, defined in Eq. (3). The diffraction gain due to the presence of a knife-edge, as compared to the free space E-field, is given by:

$$G_d(dB) = 20log\,|F(v)|. \tag{5}$$

According to Eq. (3), d_1 and d_2 have symmetric effects on v. That means that when an object stands at the symmetrical position, the Fresnel-Kirchoff diffraction parameter v will remain the same. Thus, the diffraction gain remains the same. That is, SSP2 holds.

B. Experimental Validations

In addition to the theoretical analysis, we also conducted experiments using MICAZ [29] nodes to validate SSPs.

Specifically, we used 4 m node distance to balance the localization accuracy and the costs of both the equipment and communication. The monitoring area was equally divided into 7×12 grids with the length of 0.5 m and the grids formed 4 symmetrical sub-areas. The coordinates of the transmitter and receiver are $(A, 6)$ and $(G, 6)$, respectively. The object (a human being, in our experiments) was placed at the individual grids and 100 RSS measurements were collected from each grid (as shown in Fig. 2(a)). Fig. 2(b) shows the RSS distribution when the object appeared at different locations. The RSS value is quite large as the object is close to the center. From Fig. 2(b), we observe that the RSS values follow SSP2. That is, the RSS values are kept the same for the pair of symmetrical grids. We also observe SSP3 — the RF effect is negligible when the object is more than 1 m away from the LOS. We can obtain the effective width, which is about 2.5 m. Therefore, the effective coverage area at distance of 4 m is around 3.5 m × 2.5 m. Furthermore, we tested the effective coverage width at different node distances. As shown in Fig. 2(c), we plot the RSS distribution of the Y-axis (Fig. 1) with node distance varying from 2 m to 8 m. We can set a threshold μ to intercept it, which denotes the coverage width for a given distance. More specifically, the thresholds are more than 1 m, 2 m, 3 m, 4 m at distance of 2 m, 4 m, 6 m, 8 m, respectively. Overall, our experiments demonstrate that the RSS distribution obeys the three derived SSPs in the last subsection.

According to the theoretical analysis and realistic experiments, we are motivated to locate the object based on SSP1. On
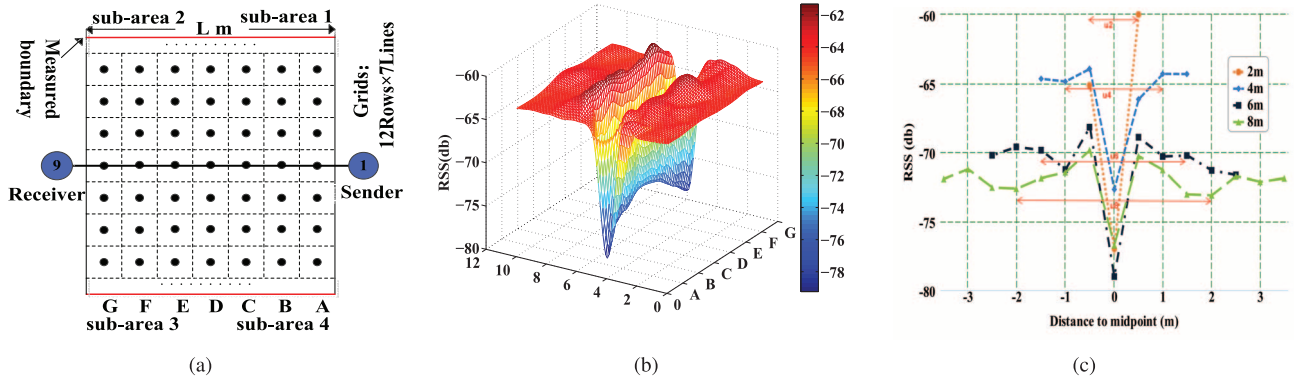
Fig. 2. (a) The distribution of sampling sites for 4 m transmitter-receiver distance. (b) RSS distribution of 4 m transmitter-receiver distance. The different gray scales represent different RSS values. The RSS values are almost the same in a pair of symmetrical grids about the area center. (c) RSS distribution of the Y-axis at different node distances.
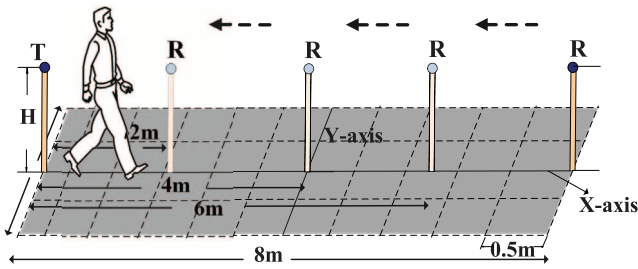

Fig. 3. Moving the receiver to different locations to extract the RSS value at different node distances.

the other hand, the information from one single link cannot suffice to locate the object accurately, because of SSP2 and SSP3. Thus, multiple links are required to achieve high localization accuracy.

To better understand the RSS fluctuation caused by the diffraction, we deployed a transmitter and a receiver, and then we moved the receiver to different locations in the 2D plane, as shown in Fig. 3. In our experiment, the receiver was moved from 8 m to 2 m along the X-axis. For each receiver location, the target object was placed at individual grids and 100 RSS measurements were collected from each grid. Fig. 4 shows the heatmap of these RSS values under the different distances from the transmitter and the receiver. It is obvious that the RSS variation value is quite large as the object is close to the center for all distances. We also observe that the RSS values follows SSP2. That is, the RSS values are kept the same for the pair of symmetrical grids. Then, the SSP3 also holds — the affected area by the diffraction is limited.

We next conducted simulations on a pair of the transmitter and receiver (i.e., a link), in order to reveal the diffraction patterns and also validate the above-mentioned theoretical model. In this simulation, the object is assumed to be a rectangle with the width of 0.5 m and the height of 1.75 m (It is the same size as that in experiments). We fixed the transmitter and placed the receiver at different locations to form different node distances. Thus, given a node distance, the monitoring area of the link is divided into several grids with the length of 0.5 m. Then, we calculated the diffraction patterns when the object stood in different 2D grids according to the theoretical models in
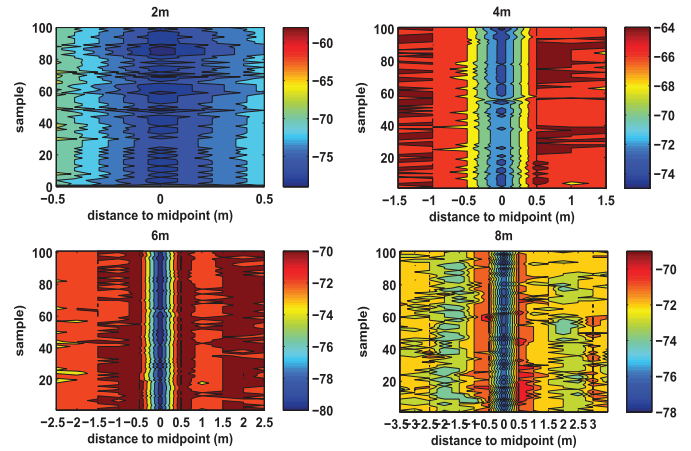

Fig. 4. The RSS distribution of different node distances.

Section III-A (see Eq. (1) to Eq. (5)). Specifically, in this simulation, the node distance is between 2 m to 8 m. The reason is that according to our experiments, when the distance is greater than 8 m or less than 2 m, the RSS fluctuations for this type of sensor are too weak to distinguish the different locations of the object (the detailed description is shown in Section IV-B3). We also used Matlab R2010a software to implement this simulation. Then we used the same setting in experiments and referred to the object as a human. In order to observe the diffraction patterns more clearly, we plot the heatmaps of RSS values obtained with both experiment and simulation at different distances.

Fig. 5(e), Fig. 5(f), Fig. 5(g) and Fig. 5(h) show the theoretical RSS distribution results at node distance of 2 m, 4 m, 6 m and 8 m. In fact, we have also simulated other distances and the RSS distribution properties are similar. As shown in Fig. 5, we observe that the experimental RSS distributions are similar to the theoretical values. It is obviously that the RSS values are kept the same for the pair of symmetrical grids and the affected area by the diffraction is limited, obviously verifying SSP2 and SSP3 again. In particular, we observe that the experimental heatmaps of RSS values are more similar to the simulation results when the node distances are 2 m and 4 m, respectively. That means when the distances are relatively short, the experimental result (diffraction patterns) is much closer to
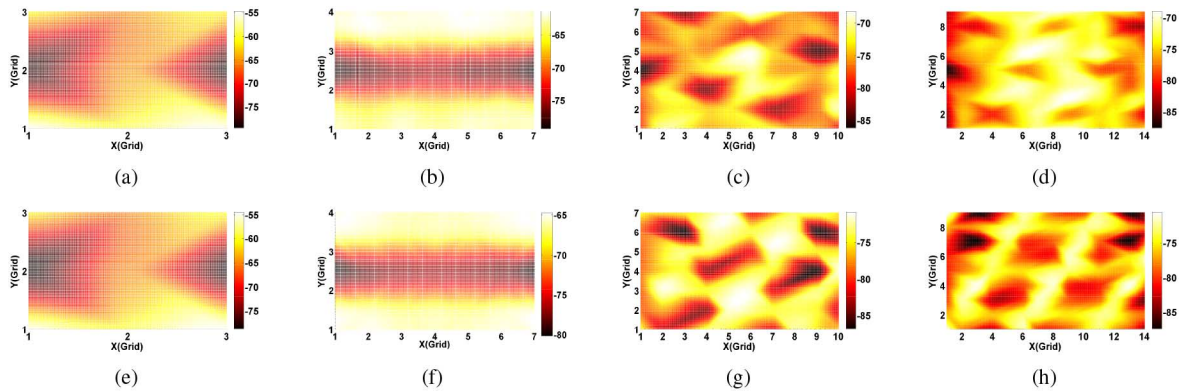
Fig. 5. Experiment and simulation results of RSS distribution at different distances. Here, (a), (b), (c), (d) show the experimental RSS distributions (diffraction patterns) at distance of 2 m, 4 m, 6 m and 8 m, respectively, while (e), (f), (g) and (h) are the corresponding simulation RSS distributions. In these figures, the x-axis and the y-axis are the ID of the 2D grids and different colors represent different RSS values (diffraction patterns) in that grid. For example, when there is no object, the RSS value keeps -63 dB and -56 dB for 4 m and 2 m distance, respectively. When the object presents, the RSS values will fluctuate.
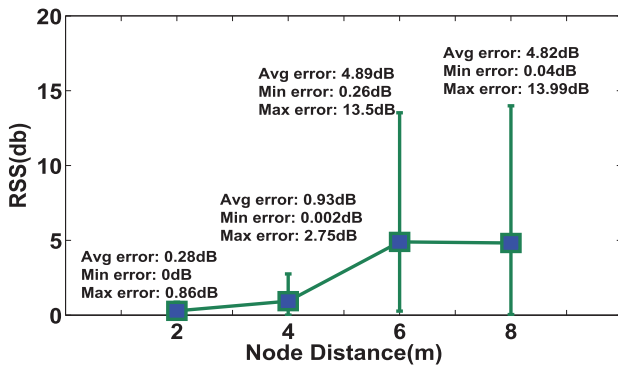

Fig. 6. RSS Errors between the theoretical model and experimental results.

the theoretical model. If the node distance becomes larger, such as 6 m or 8 m, the experimental heatmaps of RSS values are not exactly the same as the simulation results. The reason is that when the distance is larger, the RSS fluctuations caused by a human for this type of sensor become weak and are more easily disturbed by noise, which will lead to RSS deviation from the theoretical (simulation) one. Nevertheless, the experiment and simulation results are close to each other.

The RSS errors between the theoretical and experimental results at different node distance are shown in Fig. 6. Obviously, the error increases as the node distance increases. For example, the average errors are 0.86 dB and 0.93 dB for 2 m and 4 m distance, respectively, while the average errors are 4.89 dB and 4.82 dB for 6 m and 8 m, respectively. That is why the localization and tracking accuracy of 6 m and 8 m distance is lower than that of 2 m or 4 m (kindly see the Performance Evaluation in Section IV and V). On the other hand, in our testbed, the RSS values for this type of sensor nodes will have a fluctuation of plus or minus 1 dB (or 2 dB) even without any object. That is, the small RSS error shown in Fig. 6 is tolerable for localization.

IV. UNIT LOCALIZATION MODEL (ULM)

In this section, we put forward a novel multi-link based unit localization model (ULM), aiming at high localization accuracy. The whole monitoring area is composed of a number of

ULMs, each of which is to locate the object in a sub-area by several links.

First, ULMs should achieve a complete coverage of the whole monitoring area. According to the disc model [30], we can describe this issue as: how many circles are needed to provide complete coverage in a 2D plane. It is obvious that regardless of the size of the circle, it is unable to achieve complete coverage without overlapping (as shown in Fig. 7(a)). Thus, we consider regular polygon instead of circle to cover the area. Suppose that the structure of the ULM is a regular polygon with n edges. Therefore, we have three possible structures for ULM (as shown in Fig. 7(b)) to achieve a complete coverage in a 2D plane, which can be explained by the following theorem. The proof of the theorem can be found in the appendix.

Theorem 1: [31] The regular same-size polygons that can provide complete coverage are triangle, square or hexagon.

First, we will analyze the effective coverage of different structures based on the signal symmetry properties described in Section III — SSP3: The affected area of one single link is quite limited. As shown in Fig. 7(c), an approximate ellipse region represents the effective coverage of each link for detecting the object. For the triangle structure, three ellipses can cover the whole triangular monitoring area, leaving no monitoring blind area. Nevertheless, for the square structure, four ellipses form the effective detecting area, leaving one monitoring blind area in the center of the square. Thus, if the object was standing in this area, we would not be able to detect it. By analyzing the performance of RSS coverage, we chose the triangle as the ULM. In addition, by comparing square and hexagonal grids, triangles can minimize the communication cost to cover an area (in Fig. 7(c), triangles need fewer nodes and fewer communication links). The communication cost is proportional to the product of the number of nodes and the inverse of the path loss. Besides, more communication costs will lead to more energy costs. Thus, the triangle is the best choice for the ULM.

To validate and quantify the efficiency of the triangular structure, we compared it with the square and hexagonal structures. In this experiment, we set the side length to be 4 m for each structure and we randomly selected 200 samples. (Details of the experimental setup and the evaluation are the same as those
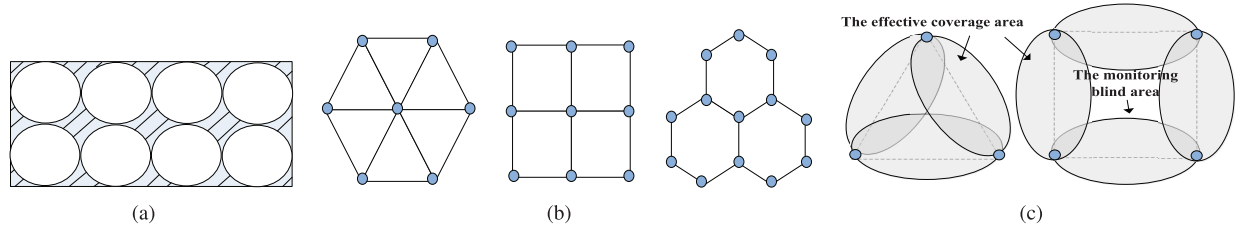
Fig. 7. (a) Covering a $2D$ plane with a circle. It cannot provide complete coverage, as shown by the shadow region. (b) Possible structures of the ULM. (c) The effective coverage of different structures.
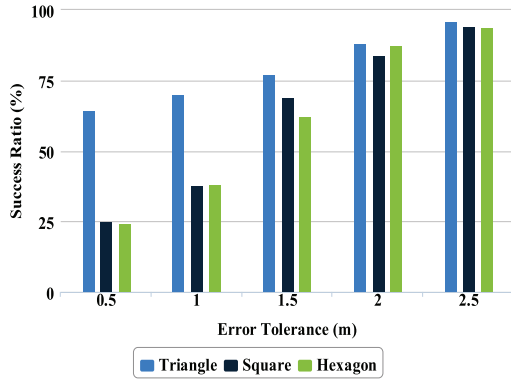

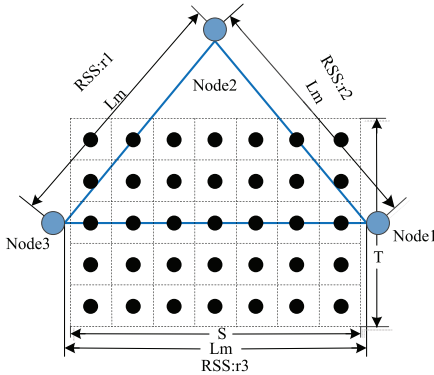Fig. 8. Success Ratio under different structures of ULM.

Fig. 9. The structure of the ULM.

Fig. 10. RSS distribution of y-lines for a 4 m ULM.

in Section IV-B) The localization results are shown in Fig. 8. Obviously, the triangular structure outperforms the other two options, especially when the error tolerance is small (e.g., below 2 m). When the error tolerance increases, the gain becomes smaller, again, indicating that the triangular structure is efficient for high localization accuracy.

According to the above analysis, we chose the triangle structure in the ULM. Also, considering Section III-B, the effective coverage area with the node distance of 4 m is around 3.5 m × 2.5 m. That is, three links are able to cover the whole area of the triangle. Thus, in this paper, each ULM is composed of three links to locate the object in this sub-area, as shown in Fig. 9. Next, we present the details of the model construction with various node distances.

A. Model Construction

Fig. 9 shows an example of the ULM, where we divide the area covered by a link into $S \times T$ grids. The proposed
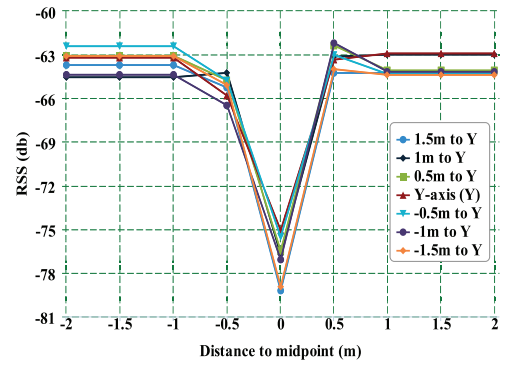
localization approach RDL uses the Bayes classifier to obtain the object's location, given the RSS vector from three links.

Let L denote the set of locations and R denote the set of the RSS values. When an object moves into the monitoring region, let $\hat{r} = [r_1, r_2, r_3]$ be the RSS vector of the three links. The posterior probability that the object is at location $l \in L$ can be calculated by:

$$P(l|\hat{r}) = \frac{P(\hat{r}|l)P(l)}{P(\hat{r})}. \tag{6}$$

The estimated location l is the one that maximizes the probability $P(l|\hat{r})$; i.e.,

$$\arg \max_l P(l|\hat{r}) = \arg \max_l P(\hat{r}|l) \frac{P(l)}{P(\hat{r})}. \tag{7}$$

We assume that all locations are of equal probability, and thus, $P(l)$ is a constant and therefore Eq. (7) is equivalent to:

$$\arg \max_l P(l|\hat{r}) = \arg \max_l P(\hat{r}|l). \tag{8}$$

Thus, the key is to obtain the priori probability $P(\hat{r}|l)$ in Eq. (8) at the training phase. However, due to different application requirements, the node distance can be different. It is obvious that a larger distance means more grids, since the length of each grid is fixed. Thus, it is difficult and time-consuming to obtain the prior probability of the RSS distribution for a large node distance. We expedite the procedure to obtain $P(\hat{r}|l)$ as follows:

It is observed that for a given node distance, the RSS values of each y-line have similar distributions. Taking a 4 m distance for example, as shown in Fig. 10, the RSS is low when the object stands at the midpoint of each y-line, while it becomes larger as the object is further away from the midpoint, implying
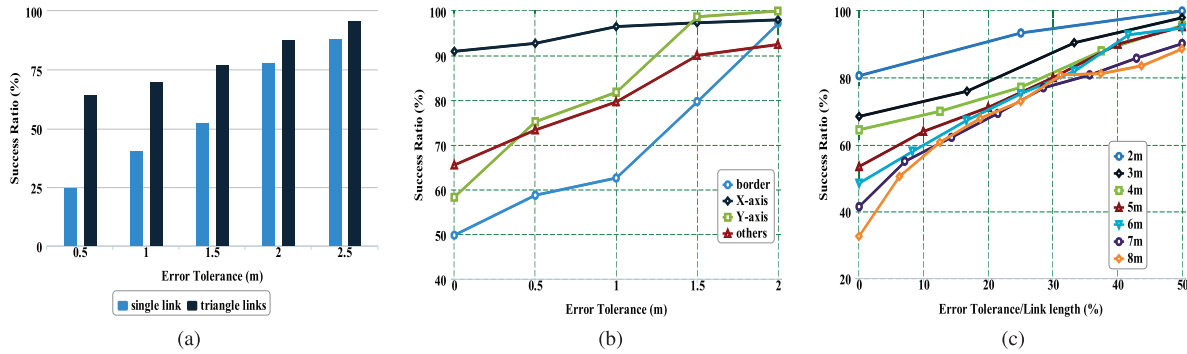
Fig. 11. (a) Localization accuracy for different numbers of links. (b) Localization accuracy for different positions. (c) Localization accuracy for different node distances.

that the RSS distribution of all the y-lines can be considered as the translation or stretching of the Y-axis.

For a given node distance, let $f(.)$ represent the relationship between the RSS values and the grid locations; i.e., $r^{(i)} = f(Lg^{(i)})$, $1 \leq i \leq k$, where $Lg : \{Lg^{(i)} = (x^{(i)}, y^{(i)})\}$ is the set of grid locations for the i-th y-line and $r : \{r^{(i)}\}$ is the set of RSS values corresponding to $Lg^{(i)}$, and k is the number of y-lines. Thus, the RSS transformation from the Y-axis (L_{MVL}) to the i-th y-line ($L_{VL}^{(i)}$) can be expressed as:

$$f_{VL}^{(i)} = \alpha^{(i)} f_{MVL} + \beta^{(i)}, \qquad (9)$$

where $\alpha^{(i)}$ and $\beta^{(i)}$ denote the correlation coefficients of the transformation. Therefore, for a given distance, the priori probability of RSS distribution can be constructed by transforming the measurements from the Y-axis to each y-line without reliance on the testing of each grid. By doing so, we make the whole procedure much simpler.

B. Performance Evaluation

We deployed MICAZ [29] nodes with Chipcon CC2420 and set the radio frequency to 2.4 GHz. The transmission power is 0 dB, and the sender sends a packet periodically to the receiver. The packet includes a byte node id, four bytes voltage, four bytes RSS and four bytes packet number. When the receiver receives the packet, it can derive the RSS data and then send this record to the datacenter. All the sensors were placed at the height of 0.95 m on the playground of Northwest University. Because 0.95 m performs better according to our experiment. We set the sampling period as 2 seconds to avoid severe packet losses or communication collisions. Volunteers stood at the given locations for a period of time and we made the measurements. The RSS values of each node were recorded during the experiment. The details of the experiments are posted online at the following website http://219.245.18.73/lab/. (Please click 'Our Experiment -> Data'). RDL used a triangle deployment with 4 m node distance to receive RSS at three different locations forming an RSS vector. We evaluated its localization accuracy and compared it with the single link deployment. Then, we evaluated whether or not it was robust and scalable with different node distances. To better understand RDL, we compared it with the Midpoint algorithm and the Intersection

algorithm [13] under both the sparse and dense deployments. For a fair comparison, all three algorithms used the same triangle deployment.

Since all node locations are known, the object's location (x_i, y_i) can be estimated by ULM when it moves into the monitoring area. We define the error tolerance as the maximum error in location distance that the system can tolerate to assist the evaluation of the localization results. If we can accept the estimated location to be at most $k - 1$ grids away from the true object location, the error tolerance equals $k \times l$, where k is a positive integer and greater than 1, and l is the grid length. For example, in our experiment, l is 0.5 m, if we set k to be 3, the errors tolerance is 1 m. Given the error tolerance, we can calculate the percentage of the estimations that have errors below the error tolerance, named success ratio.

1) Localization Based on Multiple Links: According to the SSPs in Section III, a single link is insufficient for high localization accuracy. To evaluate the localization accuracy of RDL, we compare our triangular topology with the single link. We also chose a 4 m distance and the Bayes classifier.

As shown in Fig. 11(a), the localization accuracy is significantly improved compared with the single link, especially when the error tolerance is less than 1 m. For instance, when the tolerance is 0.5 m, the improvement is 39.5% in terms of the success ratio. The improvement becomes smaller as the error tolerance is larger, which is explained by the success ratio becoming significantly high when the error tolerance is very high. The experimental result indicates that multi-link is preferred for the high localization accuracy requirement scenario. In contrast, considering the cost of the equipment and the limited energy of sensor nodes, the single-link based approach is practical for coarse-grained localization.

2) The Impact of Location Diversity: In this subsection, we evaluated the capability of our model at different positions. Taking ULM at a distance of 4 m for example, we tested the following scenarios: object positions at the border of the covered area, the X-axis, the Y-axis and other grids. For each position, we took 100 samples randomly and the success ratio is shown in Fig. 11(b).

Specifically, RDL achieves a success ratio of 49.8%, 58.3%, 65.5%, and 90.9%, respectively. The success ratio at X-axis locations is the highest. When the error tolerance is 2 m, all positions present the similar success ratio, between 90% and
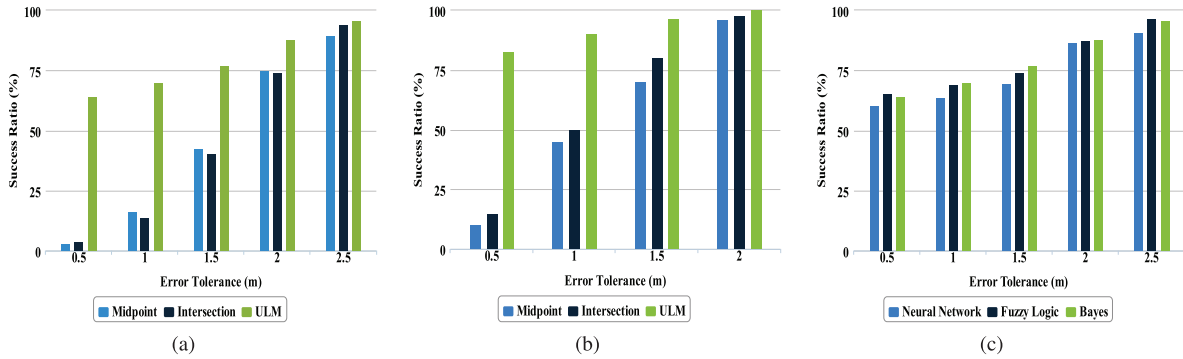
Fig. 12. (a) Algorithm comparison at the 4 m node distance. (b) Algorithm comparison at the 2 m node distance. (c) Comparison of different techniques used in ULM.

100%. According to our SSPs, the effective coverage area of each link is limited. That is why the success ratio at border positions is lower than that of the X-axis positions.

3) The Impact of Node Distance: To evaluate RDL's scalability, we ran experiments at different transmitter-receiver distances (from 2 m to 8 m with a step size of 1 m). The average success ratios for the ULM at different node distances are shown in Fig. 11(c). We can see that the larger the node distance, the lower the localization accuracy. This is explained by the RSS becoming weaker as the distance increases, so that it is more prone to errors due to noise and other interfering sources. Meanwhile, as the node distance increases, it becomes difficult to identify each grid using the RSS distribution. If the error tolerance is 0.5 m, the success ratio is 80.6%, 68.4%, 64.25%, 53.5%, 48.14%, 41.4%, and 32.55% for 2 m, 3 m, 4 m, 5 m, 6 m, 7 m and 8 m node distances, respectively. Nevertheless, a shorter node distance indicates more nodes to be deployed. That is, a tradeoff exists between localization accuracy and the costs of both the equipment and communication. For example, although the success ratio of 4 m is 16.35% lower than that of 2 m, the deployment cost of 2 m is 50% higher than that of 4 m. Specifically, 4 m is a good choice for the tradeoff between accuracy and cost. Actually, according to our experiments, when the distance is greater than 8 m or less than 2 m, the RSS fluctuations for this type of sensor are too weak to distinguish the different locations of the object. Thus, the upper and lower bounds of the node distance for this type of sensor are 8 m and 2 m, respectively.

4) Comparison of Existing Algorithms in Both Sparse and Dense Deployment: We compared RDL with the Midpoint algorithm and the Intersection algorithm in [13]. For fair comparisons of the three algorithms, we set the node distance as 4 m, because the node distance in the Midpoint algorithm and the Intersection algorithm has to be fixed. Given the fixed monitoring region, 4 m is a relatively sparse deployment, compared to the setup in [13]. All of the three algorithms used the same triangle deployment to receive RSS at three different locations. All of the nodes were placed at the height of 0.95 m on the playground at Northwest University. We set the sampling period as 2 seconds to avoid severe packet losses or communication collisions. Volunteers stood at the given locations for a period of time as we did the measurements. The RSS values for each node were recorded for the data center during the

experiment. We randomly selected 200 samples from the measurements for each algorithm. Fig. 12(a) illustrates the average results. We found that, in terms of the localization accuracy, the proposed RDL outperformed both the Midpoint and the Intersection algorithms, especially when the error tolerance was less than 1.5m.

To better understand RDL, we compared it with the other two algorithms under a dense deployment to see whether or not it is applicable to both the sparse and dense deployments. Thus, we changed the side length of the triangle to 2 m, which is the same distance as used in [13], and the localization results are shown in Fig. 12(b). We observe that RDL still outperforms the Midpoint algorithm and the Intersection algorithm. This indicates that RDL can locate the object accurately in both the sparse and dense deployments, in comparison to the state-of-the-art algorithms.

5) Impact of Different Techniques: In this paper, we mainly adopt Bayes classifier to obtain the estimated locations based on their RSS vector from the triangle ULM. In fact, to assist the proposed RDL, we can also use other techniques such as fuzzy logic [32]–[35] or neural network (NN) [36]–[39] to replace Bayes classifier to achieve satisfactory performance. These techniques are chosen since they are classical techniques which show good results in this kind of problems. In addition, these algorithms have similar features (e.g. classification and prediction) as Bayes. We implemented Bayes classifier using Matlab R2010a software according to the technique mentioned in Section IV-A. Fuzzy logic and neural network are implemented using the methods in [35] and [38], respectively.

In this experiment, the scenario is an outdoor playground using the ULM at 4 m node distance. The results of the three techniques are shown in Fig. 12(c). It is obviously that the performance of "Fuzzy Logic" is similar to that of "Bayes" no matter what the error tolerance is. In some cases, "Fuzzy Logic" even outperforms "Bayes" slightly. For example, the success ratio of "Fuzzy Logic" is 1.14% and 1% higher than that of "Bayes" when the error tolerance is 0.5 m and 2.5 m, respectively. Neural network also has the similar performance.

However, both fuzzy logic and neural network require the user to set appropriate parameters in order to achieve better success ratio, which increases the extra complexity in applications. In contrast, the proposed method in this paper only needs to consider the probability formula of Bayes (using the

idea described in Section IV-A). Thus, in the following, we adopt Bayes considering its simplicity and how to apply more advanced fuzzy logic, neural network, or other technologies to further improve the performance remains an important future research issue.

V. TRACKING APPLICATION

In tracking applications, such as intrusion detection and wildlife monitoring, we need to obtain the trajectory of the moving object. In this section, we discuss how RDL helps to track the moving object. In addition, we conduct extensive experiments to show its effectiveness. We begin by presenting some notations.

1) *Contribution Links*: are the links whose RSS is beyond the threshold. Here, the threshold indicates that an object is present in the monitoring region covered by the link.
2) *Contribution Nodes*: are the nodes that are associated with the Contribution Links. We define the Contribution Node Set as CNS for short.
3) *Contribution ULM*: is used to locate the object; i.e., the effective ULM.

The moving trajectory identification includes two phases: the offline phase and the online phase. During the offline phase, we construct ULMs, and the possible locations (x_i, y_i) can be estimated by these ULMs, as discussed in Section IV. In the online phase, when the object moves into the monitoring region, we first eliminate the environment noise from the raw RSS and find the Contribution Nodes. Next, we find the Contribution ULMs and identify the moving trajectory.

A. The Moving Trajectory Identification

Our approach to moving trajectory identification is performed in three steps. In the first step, we eliminate the environment noise in the obtained RSS vector via RSS preprocessing. In step two, we identify the effective Contribution Nodes for precise tracking. In the last step, we identify the moving trajectory by a series of locations.

1) Preprocessing: In outdoor (or wild field) tracking applications, the RSS value obtained from the sensor nodes is often affected by interference due to the environment. The direct usage of the raw RSS to identify the object's locations will lead to considerable location errors. As such, the RSS data should be preprocessed before it is used.

Let $[r_{1,LN_i}, r_{2,LN_i}, \ldots, r_{n,LN_i}]$ be the RSS sequence of node N_i during time period n, and its corresponding link is LN_i. We call this sequence the r-sequence. If any RSS value is beyond its threshold; i.e.,

$$r_{j,LN_i} > r_i, 1 \le j \le n, \tag{10}$$

then the link LN_i is a possible Contribution Link and node N_i is a possible Contribution Node. Here, r_i is the RSS threshold. To simplify the calculation, we also introduce b-sequence (a binary value sequence): $[b_{1,LN_i}, b_{2,LN_i}, \ldots, b_{n,LN_i}]$. More specifically, if r_{j,LN_i} is greater than r_i, then $b_{j,LN_i} = 1$, otherwise $b_{j,LN_i} = 0$. We define $[N_1, N_2, \ldots, N_g]$ as the initial CNS, where $1 \le g \le n$.
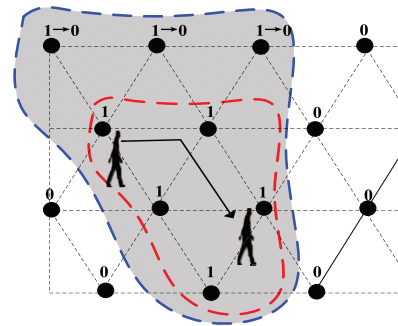

Fig. 13. Identifying the Contribution Nodes.

After data preprocessing, two kinds of RSS sequences occur: the b-sequence is used to precisely identify the Contribution Nodes, and the r-sequence is used to estimate the object's location. Next, we will introduce how to use the b-sequence to identify CNS and the effective ULM.

2) Precisely Identifying the Contribution Nodes: A link could be mistaken as a Contribution Link (based on equ. (10)) due to environment noise. Often, the RSS fluctuations will continuously appear for a period when the sensor node is located for the trajectory of a moving object; otherwise, the RSS fluctuation appears with small peaks due to the noise. To avoid the false positive, our first step is to scan the initial CNS and sort the identified Contribution Nodes based on the affected time length. To that end, we observe that the number of '1's in the b-sequence exactly presents the time duration. For each possible Contribution Node, when the number of '1's in the b-sequence is less than a given threshold u (it relies on different application requirements), we consider that the RSS fluctuations come from the environmental noise.

$$\sum_{j=1}^{n} b_{j,LN_i} \le u \tag{11}$$

According to equ. (11), those nodes whose number of '1's in their b-sequence is less than u are then removed from the initial CNS. As such, we obtain the updated CNS $[N_1, \ldots, N_i, \ldots, N_k], k \le g$.

Fig. 13 shows an example. When an object moves into the monitoring region, the initial CNS can be identified based on Equ. (10). The nodes in the large dotted circle area are the initial CNS, while the RSS fluctuations caused by the moving object exist in a very limited region de facto. Equ. (11) allows us to have a more precise CNS (shown within the small dotted circle area), as well as effective ULMs.

3) Trajectory Identification: After mitigating the effect of environment noise, we next focus on tracking the moving object only. After all the nodes in CNS have been sorted descendingly by the time duration, we start from node N_1 and scan all the other nodes in the CNS. If nodes such as N_j and N_s exist, a triangle can be constructed with node N_i, where $i < j, s \le k$. These three nodes construct a ULM and we mark the nodes as the effective Contribution Nodes. The process is repeated, until all nodes are marked.

For each Contribution ULM, compared with the b-sequences of nodes in the triangle, we choose the node with the b-sequence
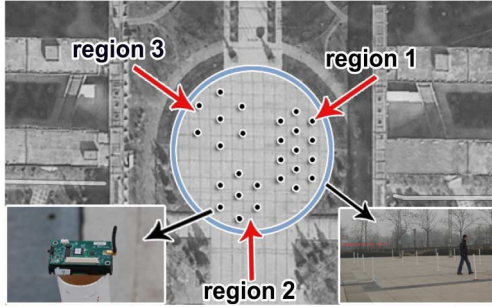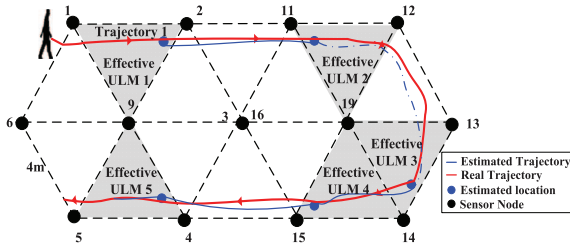
Fig. 14. Deployment of the sensor nodes.

Fig. 16. Estimated trajectory 2 at a distance of 4 m.

Fig. 15. Estimated trajectory 1 at a distance of 4 m.

TABLE I
LOCALIZATION RESULTS FOR TRAJECTORY 1

ID of effective ULM	1	2	3	4
X coordinates	G	G	D,E	E,F
Y coordinates	4	4	4,3	2,3

TABLE II
LOCALIZATION RESULTS FOR TRAJECTORY 2

ID of effective ULM	1	2	3	4
X coordinates	G	G	D,E	E,F
Y coordinates	4	4	4,3	2,3

TABLE III
LOCALIZATION RESULTS FOR ULM (A) 6M NODE DISTANCE
(B) 8M NODE DISTANCE

(a) 6m node distance

ID of effective ULM	1	2	3	4	5
X coordinates	F,J	F	F	I	J
Y coordinates	4,4	3	5	5	6

(b) 8m node distance

ID of effective ULM	1	2	3	4	5
X coordinates	H,K	N	H	G	F,J
Y coordinates	8,4	6	8	8	4,4

having the largest number of '1' as the corresponding node of r_3 in the RSS vector $\hat{r} = [r_1, r_2, r_3]$. By doing so, the corresponding r-sequences of the three nodes constitutes the RSS vector $\hat{r}$. Then, we divide $\hat{r}$ into several pieces, and each piece contains the RSS values with a fixed window size w. Then we can obtain the object's location at time w using the average RSS of the piece, based on ULM. Finally, by combining the results of each piece, we have the trajectory during period n.

B. Experiment Evaluation

1) Experiment Setup: We deployed MICAZ [29] nodes on the playground of Northwest University. As shown in Fig. 14, three regions are present with a total size of 28 m × 25 m. The experiments were repeated at various node distances ranging from 4 m to 8 m. More specifically, 14 nodes were sparsely distributed in the first region and used to construct two regular hexagons with a distance of 4 m between neighboring nodes. For the second region, we deployed 6 nodes, which were used to construct 1 regular hexagon at a distance of 8 m. In the last region, we also deployed 6 nodes at a distance of 6 m. We divided each monitoring region into several grids and denoted the horizontal direction as the x-axis, and the vertical direction as the y-axis. The X coordinates are: $A, B, C, \ldots$ from right to left, while Y coordinates are: $1, 2, 3, \ldots$ from bottom to top. Thus, the coordinate of each grid is $A1, A2, \ldots$. Our goal is to evaluate the tracking performance with different moving trajectories and at different node distances. We set the sampling period as 2 seconds to avoid severe packet losses or communication collisions. We asked volunteers to walk through the sensor node array with various trajectories. The RSS values of each node were recorded during the experiment.

2) Results for the 4 m Node Distance: In Figs. 15 and 16, the object moves along the two red curves and the moving speed is around 0.93 m/s. Based on step 2 of the moving trajectory
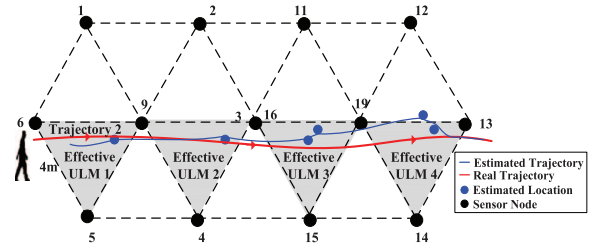
identification in Section V-A2, we find five effective ULMs for trajectory 1. The localization results are shown in Table I and in Fig. 15. The trajectory is obtained by connecting all of the estimated locations. Note that the estimated trajectory is close to the ground truth. Interestingly, we find that the estimated locations are sparse, especially between node 12 and node 13. This is explained by the object's moving speed, which is faster than the sampling frequency of the nodes.

Table II shows the results when the object moves along trajectory 2. In this case, we find four effective ULMs to estimate the object's locations. Interestingly, two coordinates are possible for the effective ULMs 3 and 4. This happens because the object does not have a uniform motion. Specifically, when the object moves into these positions, its speed is slow, which leads to a long time interference. Thus, we can obtain two different location coordinates. Fig. 16 shows the estimated moving trajectory.

3) Results of 6 m/8 m Node Distance: In this subsection, the object moves along the boundary of the monitoring region and the moving speed is about 0.93 m/s. We find a total of five effective ULMs and Table III(a) shows the estimated object's locations at different times. We observe that effective ULM 1 involves two location coordinates, similar to Section V-B2. The estimated trajectory is shown in Fig. 17(a), and some packet loss also takes place. The object is moving fast when it is close
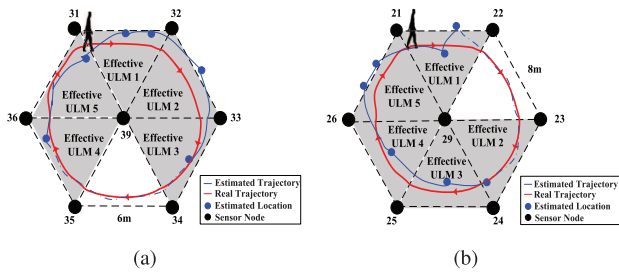
Fig. 17. (a) The estimated trajectory at a distance of 6 m. (b) the estimated trajectory at a distance of 8 m.
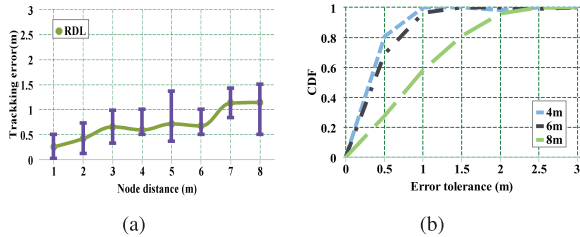

Fig. 18. (a) Tracking error for different node distances. (b) CDF of tracking error for different node distances.

to the link for node 34 and node 35. This experiment indicates that our method can be applied to a 6 m node distance as well.

Next, we choose the node distance of 8 m. Table III(b) shows the localization results for five effective ULMs and the estimated trajectory is shown in Fig. 17(b). We observe that the localization accuracy is low with a long node distance. This is explained by the number of grids that become larger as the node distance becomes longer. In addition, no significant differences in RSS values are seen among the different grids, which could lead to a reduced localization accuracy.

4) Discussion: We define average tracking error as the average error between the estimated locations and the real locations for the whole trajectory. We ran further experiments at distances of 1 m to 8 m. Fig. 18(a) shows the average tracking errors at different node distances. The tracking error was found to increase as the node distance becomes larger. More specifically, when the node distance is 4 m, the average, minimum, and maximum tracking errors are 0.59 m, 0.5 m and 1 m, respectively. When the node distance is 8 m, however, the tracking errors are 1.14 m, 0.5 m, 1.5 m, respectively. Furthermore, Fig. 18(b) plots the comparison of three different node distances. Apparently, the tracking errors at 4 m and 6 m are lower than those at 8 m. This also confirms that the tracking error for RDL increases as the node distance increases. However, our model can maintain sufficient accuracy on average for tracking applications.

VI. CONCLUSIONS AND FUTURE WORK

In this paper, we proposed RDL as a simple yet effective approach for RSS-based passive object localization. We analyzed the RSS distribution properties at a variety of node distances, using intensive measurements and diffraction theory. We also found that the structure of the triangle is efficient for low-cost localization, and we constructed a unit localization

model for high localization accuracy. In addition, we showed a tracking application to identify the trajectory of the moving object. Extensive experiments have shown that RDL can improve the localization accuracy by more than 50% when the error tolerance is less than 1.5 m, compared to existing approaches. The estimated trajectory is close to the ground truth.

RDL can be applied to different node distances; however, it needs to obtain the priori probability $P(\hat{r}|l)$ at each distance. Therefore, can we transfer the RSS distribution of L m m to L' m, with the aim of simplifying the procedure? Besides, given the other non-deterministic factors in an outdoor environment with many wireless sensor nodes being deployed, more experimental and analytical works are needed for the localization, especially in dynamic and complex environments where the channel conditions might change. In addition, identifying and localizing multiple objects is an interesting and challenging research topic. As our focus is to solve passive localization in outdoor situations, our experiments took place in the playground of Northwest University, which does not have a rich multi-path environment. Thus, we only need to consider diffraction. To evaluate the feasibility of the proposed RDL method in the indoor environment, the multi-path effect needs to be further investigated. Furthermore, the data gathering strategy [40] should be also considered when using in large-scale networks. We leave these interesting issues for future studies.

APPENDIX A

Proof: The angle sum of an arbitrary polygon can be computed by:

$$(n - 2) \times 180, \tag{12}$$

where n is the number of the edges. Thus, the size of each angle is:

$$((n - 2) \times 180)/n. \tag{13}$$

To provide complete coverage in the whole monitoring area, taking a vertex of an arbitrary polygon as the center, the total number M of polygons, which are needed to cover the $2D$ plane, is:

$$M = \frac{360}{\frac{(n-2) \times 180}{n}} = \frac{2n}{n - 2}. \tag{14}$$

Here, the range of n is 3, 4, 5, 6, ... Obviously, when n is 3, the total number of polygons is 6. When n is 4 and 6, the total number is 4 and 3, respectively. When n equals 5, the total number is not a positive integer. When n is greater than 6, Eq. (14) can be transformed into the following:

$$M = \frac{2n}{n - 2} = \frac{2}{1 - \frac{2}{n}}. \tag{15}$$

We observe that M decreases as n increases. Thus, when n is greater than 6, no proper positive integer solution exists for M. Therefore, the possible polygon is a triangle, square, or hexagon. □

REFERENCES

[1] L. M. Ni, Y. Liu, Y. C. Lau, and A. P. Patil, "LANDMARC: Indoor location sensing using active RFID," *Wireless Netw.*, vol. 10, no. 6, pp. 701–710, 2004.

[2] P. Bahl and V. N. Padmanabhan, "Radar: An in-building RF-based user location and tracking system," in *Proc. IEEE InfoCom*, 2000, pp. 775–784.

[3] P. Bahl, V. N. Padmanabhan, and A. Balachandran, "Enhancements to the radar user location and tracking system," Microsoft Research, Redmond, WA, USA, Tech. Rep. MSR-TR-2000-12, 2000.

[4] K. Lorincz and M. Welsh, "Motetrack: A robust, decentralized approach to RF-based location tracking," in *Proc. Location Context Awareness*, 2005, pp. 49–62.

[5] H. Nakayama, N. Ansari, A. Jamalipour, and N. Kato, "Fault-resilient sensing in wireless sensor networks," *Comput. Commun.*, vol. 30, no. 11, pp. 2375–2384, 2007.

[6] A. Oka and L. Lampe, "Distributed target tracking using signal strength measurements by a wireless sensor network," *IEEE J. Sel. Areas Commun.*, vol. 28, no. 7, pp. 1006–1015, Sep. 2010.

[7] J. Chen, K. Cao, K. Li, and Y. Sun, "Distributed sensor activation algorithm for target tracking with binary sensor networks," *Cluster Comput.*, vol. 14, no. 1, pp. 55–64, 2011.

[8] S. Yang, P. Dessai, M. Verma, and M. Gerla, "FreeLoc: Calibration-free crowdsourced indoor localization," in *Proc. IEEE InfoCom*, 2013, pp. 2581–2589.

[9] J. Wang and D. Katabi, "Dude, where's my card?: RFID positioning that works with multipath and non-line of sight," in *Proc. ACM SIGCOMM*, 2013, pp. 51–62.

[10] Y. Shu, P. Cheng, Y. Gu, J. Chen, and T. He, "TOC: Localizing wireless rechargeable sensors with time of charge," *ACM Trans. Sensor Netw.*, vol. 11, no. 3, p. 44, 2015.

[11] Y. Wen, X. Tian, X. Wang, and S. Lu, "Fundamental limits of RSS fingerprinting based indoor localization," in *Proc. IEEE Conf. Comput. Commun. (INFOCOM)*, 2015, pp. 2479–2487.

[12] D. Zhang, Y. Liu, and L. M. Ni, "Link-centric probabilistic coverage model for transceiver-free object detection in wireless networks," in *Proc. IEEE 30th Int. Conf. Distrib. Comput. Syst. (ICDCS'10)*, 2010, pp. 116–125.

[13] D. Zhang, J. Ma, Q. Chen, and L. M. Ni, "An RF-based system for tracking transceiver-free objects," in *Proc. 5th Annu. IEEE Int. Conf. Pervasive Comput. Commun. (PerCom'07), 2007*, pp. 135–144.

[14] Y. Liu, L. Chen, J. Pei, Q. Chen, and Y. Zhao, "Mining frequent trajectory patterns for activity monitoring using radio frequency tag arrays," in *Proc. 5th Annu. IEEE Int. Conf. Pervasive Comput. Commun. (PerCom'07)*, 2007, pp. 37–46.

[15] J. Kiran, H. Steven, and K. Sachin, "Pinpoint: Localizing interfering radios," in *Proc. USENIX Netw. Syst. Des. Implement. (NSDI'13)*, 2013, pp. 241–253.

[16] A. Fadel and K. Dina, "See through walls with Wi-Fi," in *Proc. ACM SIGCOMM*, 2013, pp. 75–86.

[17] O. Kaltiokallio, M. Bocca, and L. M. Eriksson, "Distributed RSSI processing for intrusion detection in indoor environments," in *Proc. ACM Int. Conf. Inf. Process. Sensor Netw. (IPSN'10)*, 2010, pp. 404–405.

[18] D. Zhang and L. M. Ni, "Dynamic clustering for tracking multiple transceiver-free objects," in *Proc. IEEE Int. Conf. Pervasive Comput. Commun. (PerCom'09)*, 2009, pp. 1–8.

[19] D. Zhang, Y. Yang, D. Cheng, S. Liu, and L. M. Ni, "Cocktail: An RF-based hybrid approach for indoor localization," in *Proc. IEEE Int. Conf. Commun. (ICC'10)*, 2010, pp. 1–5.

[20] J. Wang, D. Fang, X. Chen, Z. Yang, T. Xing, and L. Cai, "LCS: Compressive sensing based device-free localization for multiple targets in sensor networks," in *Proc. IEEE InfoCom*, 2013, pp. 145–149.

[21] X. Zheng, J. Yang, Y. Chen, and Y. Gan, "Adaptive device-free passive localization coping with dynamic target speed," in *Proc. IEEE InfoCom*, 2013, pp. 485–489.

[22] M. Bocca, O. Kaltiokallio, N. Patwari, and S. Venkatasubramanian, "Multiple target tracking with RF sensor networks," *IEEE Trans. Mobile Comput.*, vol. 13, no. 8, pp. 1787–1800, Aug. 2014.

[23] A. Saeed, A. E. Kosba, and M. Youssef, "Ichnaea: A low-overhead robust WLAN device-free passive localization system," *IEEE J. Sel. Topics Signal Process.*, vol. 8, no. 1, pp. 5–15, Feb. 2014.

[24] F. Adib, Z. Kabelac, D. Katabi, and R. C. Miller, "3D tracking via body radio reflections," in *Proc. Usenix Netw. Syst. Implement. (NSDI)*, 2014, vol. 14, pp. 317–329.

[25] J. Xiao, K. Wu, Y. Yi, L. Wang, and L. M. Ni, "Pilot: Passive device-free indoor localization using channel state information," in *Proc. IEEE 33rd Int. Conf. Distrib. Comput. Syst. (ICDCS)*, 2013, pp. 236–245.

[26] L. Liu, X. Zhang, and H. Ma, "Dynamic node collaboration for mobile target tracking in wireless camera sensor networks," in *Proc. IEEE INFOCOM*, 2009, pp. 1188–1196.

[27] L. Yang, Y. Chen, X. Y. Li, C. W. Xiao, M. Li, and Y. H. Liu, "Tagoram: Real-time tracking of mobile RFID tags to high precision using cots devices," in *Proc. ACM MobiCom*, 2014, pp. 237–248.

[28] T. S. Rappaport *et al.*, *Wireless Communications: Principles and Practice*, vol. 207. Englewood Cliffs, NJ, USA: Prentice-Hall, 1996.

[29] Memsic, 2009 [Online]. Available: http://www.memsic.com/

[30] S. J. Orfanidis. *Electromagnetic Waves and Antennas*. New Brunswick, NJ, USA: Rutgers Univ. Press, 2002.

[31] S. Zhao and Z. Zhang, "Study regular hexagonal node coverage model of wireless sensor networks," *Comput. Eng.*, vol. 36, no. 20, pp. 113–118, 2010.

[32] J. J. Astrain, J. Villadangos, J. R. Garitagoitia, J. R. González de Mendívil, and V. Cholvi, "Fuzzy location and tracking on wireless networks," in *Proc. 4th ACM Int. Workshop Mobility Manage. Wireless Access*, 2006, pp. 84–91.

[33] J. M. Alonso *et al.*, "Enhanced WiFi localization system based on soft computing techniques to deal with small-scale variations in wireless sensors," *Appl. Soft Comput.*, vol. 11, no. 8, pp. 4677–4691, 2011.

[34] L. Mengual, O. Marbán, and S. Eibe, "Clustering-based location in wireless networks," *Expert Syst. Appl.*, vol. 37, no. 9, pp. 6165–6175, 2010.

[35] T. Garcia-Valverde *et al.*, "A fuzzy logic-based system for indoor localization using WiFi in ambient intelligent environments," *IEEE Trans. Fuzzy Syst.*, vol. 21, no. 4, pp. 702–718, Aug. 2013.

[36] M. Gholamin, N. Cai, and R. W. Brennan, "An artificial neural network approach to the problem of wireless sensors network localization," *Robot. Comput. Integr. Manuf.*, vol. 29, pp. 96–109, 2013.

[37] M. S. Rahman, Y. Park, and K. D. Kim, "Localization of wireless sensor network using artificial neural network," in *Proc. IEEE Int. Conf. (ISCIT'09)*, 2009, pp. 639–642.

[38] L. Gogolak, S. Pletl, and D. Kukolj, "Indoor fingerprint localization in WSN environment based on neural network," in *Proc. IEEE Int. Conf. (SISY'11)*, 2011, pp. 293–296.

[39] N. Kubota, D. Tang, T. Obo, and S. Wakisaka, "Localization of human based on fuzzy spiking neural network in informationally structured space," in *Proc. IEEE Int. Conf. Fuzzy Syst.*, 2010, pp. 1–6.

[40] Y. Zhang, S. He, and J. Chen, "Data gathering optimization by dynamic sensing and routing in rechargeable sensor networks," in *Proc. 10th Annu. IEEE Commun. Soc. Conf. Sensor Mesh Ad Hoc Commun. Netw. (SECON)*, 2013, pp. 273–281.

Chen Liu received the B.S. and M.S. degrees in computer science from Northwest University, Xi'an, China, in 2009 and 2012, respectively. She is currently pursuing the Ph.D. degree at Northwest University. Her research interests include localization and wireless networks.

Dingyi Fang received the Ph.D. degree in computer application technology from Northwestern Polytechnical University, Xi'an, China, in 2001. He is currently a Professor with the School of Information Science and Technology, Northwest University, Xi'an, China. His research interests include mobile computing and distributed computing systems, network and information security, and wireless sensor networks.
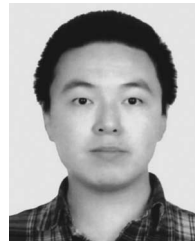
Zhe Yang received the B.S. degree in information engineering from Xi'an Jiaotong University, Xi'an, China, and the Ph.D. degree in electrical and computer engineering from the University of Victoria, Victoria, BC, Canada, in 2005 and 2013, respectively. He is currently an Associate Professor with the School of Computer Science, Northwestern Polytechnical University, Xi'an, China. His research interests include cross-layer design, scheduling and resources allocation for wireless networks, and synchronization.

Hongbo Jiang (M'08–SM'14) received the B.S. and M.S. degrees from Huazhong University of Science and Technology, Wuhan, China, and the Ph.D. degree from Case Western Reserve University, Cleveland, OH, USA, in 2008. After that he joined the Faculty of Huazhong University of Science and Technology, where he is now a Full Professor and the Department Chair of the Department of Communication Engineering. His research interests include computer networking, especially algorithms and protocols for wireless and mobile networks.
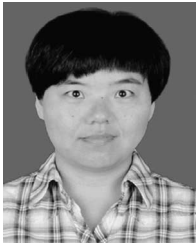
Xiaojiang Chen (M'14) received the Ph.D. degree in computer software and theory from Northwest University, Xi'an, China, in 2010. He is currently a Professor with the School of Information Science and Technology, Northwest University. His research interests include localization and performance issues in wireless ad hoc, mesh, and sensor networks and named data networks.

Wei Wang received the Bachelor's and Master's degrees in communication engineering from Xidian University, Xi'an, China, in 2000 and 2004, respectively. She is a Lecturer with Northwest University since 2004. Her research interests include wireless sensor networks and communication networks, with emphasis on design of multichannel access control and localization algorithms.

Tianzhang Xing received the B.E. degree from the School of Telecommunications Engineering, Xidian University, and the Ph.D. degree from the School of Information Science and Technology, Northwest University, Xi'an, China. He is currently an Assistant Professor with the School of Information Science and Technology, Northwest University. His research interests include wireless communication, wireless networks, with emphasis on the localization problem and the location based services.

Lin Cai (S'00–M'06–SM'10) received the M.A.Sc. and Ph.D. degrees in electrical and computer engineering from the University of Waterloo, Waterloo, Canada, in 2002 and 2005, respectively. Since 2005, she has been with the Department of Electrical and Computer Engineering, University of Victoria, Victoria, BC, Canada, and is currently a Professor. Her research interests include communications and networking, with a focus on network protocol and architecture design supporting emerging multimedia traffic over wireless, mobile, ad hoc, and sensor networks. She has served as the TPC Symposium Co-Chair for the IEEE Globecom'10 and Globecom'13, and an Associate Editor for the IEEE TRANSACTIONS ON WIRELESS COMMUNICATIONS, the IEEE TRANSACTIONS ON VEHICULAR TECHNOLOGY, *EURASIP Journal on Wireless Communications and Networking*, *International Journal of Sensor Networks*, and *Journal of Communications and Networks (JCN)*. She was the recipient of NSERC Discovery Accelerator Supplement Grants in 2010 and 2015, and the best paper awards of the IEEE ICC 2008 and the IEEE WCNC 2011.